Signal postprocessing and reflectivity calibration of the atmospheric radiation measurement program 915-mhz wind profilers

Signal Postprocessing and Reflectivity Calibration of the Atmospheric Radiation Measurement Program 915-MHz Wind Profilers

FRÉDÉRIC TRIDON AND ALESSANDRO BATTAGLIA

Earth Observation Sciences, Department of Physics and Astronomy, University of Leicester, Leicester, United Kingdom

PAVLOS KOLLIAS

Department of Atmospheric and Oceanic Sciences, McGill University, Montreal, Quebec, Canada

EDWARD LUKE

Atmospheric Sciences Division, Brookhaven National Laboratory, Upton, New York

CHRISTOPHER R. WILLIAMS

Cooperative Institute for Research in Environmental Sciences, University of Colorado Boulder, and Atmospheric Administration/Earth System Research Laboratory, Boulder, Colorado

(Manuscript received 12 July 2012, in final form 4 December 2012)

ABSTRACT

The Department of Energy Atmospheric Radiation Measurement (ARM) Program has recently initiated a new research avenue toward a better characterization of the transition from cloud to precipitation. Dual-wavelength techniques applied to millimeter-wavelength radars and a Rayleigh reference have a great potential for rain-rate retrievals directly from dual-wavelength ratio measurements. In this context, the recent reconfiguration of the ARM 915-MHz wind profilers in a vertically pointing mode makes these instruments the ideal candidate for providing the Rayleigh reflectivity/Doppler velocity reference. Prior to any scientific study, the wind profiler data must be carefully quality checked. This work describes the signal postprocessing steps that are essential for the delivery of high-quality reflectivity and mean Doppler velocity products—that is, the estimation of the noise floor from clear-air echoes, the absolute calibration with a collocated disdrometer, the dealiasing of Doppler velocities, and the merging of the different modes of the wind profiler. The improvement added by the proposed postprocessing is confirmed by comparison with a high-quality S-band profiler deployed at the ARM Southern Great Plains site during the Midlatitude Continental Convective Clouds Experiment. With the addition of a vertically pointing mode and with the postprocessing described in this work in place, besides being a key asset for wind research wind profilers observations may therefore become a centerpiece for rain studies in the years to come.

1. Introduction

For two decades, the U.S. Department of Energy (DOE) Atmospheric Radiation Measurement (ARM) Program (Stokes and Schwartz 1994) has been managing highly instrumented facilities with a large variety of collocated active (e.g., millimeter-wavelength radars or lidars) and passive (e.g., microwave sensors) at different sites (http://www.arm.gov), such as the Southern Great Plains (SGP) site in Oklahoma. These continuous atmospheric observations represent a unique dataset valuable for the study of the formation processes of clouds and their influence on climate through their radiative effect in a broad range of weather conditions.

More recently, thanks to the ARM program new-generation cloud radars (Kollias et al. 2007b), a novel research avenue has been initiated toward a better characterization of the transition from cloud to precipitation. This opportunity stems from the fact that cloud radars can be actually exploited to provide

Corresponding author address: Frédéric Tridon, Earth Observation Sciences, Department of Physics and Astronomy, University of Leicester, University Road, Leicester LE1 7RH, United Kingdom.
E-mail: f.tridon@leicester.ac.uk

DOI: 10.1175/JTECH-D-12-00146.1

a holistic view of the water cycle, since they adequately detect both cloud and precipitation (Kollias et al. 2007a). In particular, rain attenuation of cloud radars does represent a useful signal for the retrieval of precipitation characteristics. In this perspective, Matrosov (2005) and Matrosov et al. (2006) used the vertical profile of reflectivity measured by ARM cloud radars (35 GHz, 8.6 mm) to infer the rain attenuation and to retrieve rain-rate profiles, assuming that, in stratiform rain, the nonattenuated reflectivity profiles are rather constant below the melting layer. However, in the case of vertical variability of hydrometeor profiles and/or of wind-shear-tilting vertical cores of precipitation, the former assumption does not hold, and this represents the most limiting factor of the accuracy of the retrievals. To improve the accuracy of this methodology and to extend its application to most rain cases, the cloud radar reflectivity should be compared with collocated nonattenuated Rayleigh reflectivity measured by centimeter radars, as done for instance in Matrosov (2010) with the use of data from a scanning C-band radar near the tropical western Pacific ARM facility in Darwin, Northern Territory, Australia. Such measurements can also be provided by 915-MHz (33 cm) wind profilers, which are available at most of these facilities.

The 915-MHz radars are sensitive both to meteorological targets such as precipitation via Rayleigh scattering and to inhomogeneities in the air refractive index via Bragg scattering (Ralph 1995). The latter characteristic allows the retrieval of profiles of vertical and horizontal winds in clear air, while the former makes them suitable to study the vertical structure of precipitating systems. To explore their full potential for precipitation studies, the wind profilers have been recently reconfigured in a vertically pointing mode with staggered pulse repetition frequencies (PRFs) for the observation of vertical velocities in deep convective systems (P. Kollias 2011, personal communication). These modifications allow the increase of its temporal and vertical resolutions and of the maximum unambiguous Doppler velocity.

The mean Doppler velocity (first moment of the spectrum) is the essential measured parameter for wind studies (Carter et al. 1995) and has been largely used since the deployment of the wind profiler at SGP in 1993. On the other hand, the measured reflectivity (zeroth moment of the spectrum) has rarely been the focus of past studies because the wind profiler was subject to saturation, a well-known issue associated with strong signals (e.g., coming from rain and hail at close range) both for cloud radars (Matrosov 2005) and for wind profilers (Gage et al. 1999). Indeed, every radar system is capable of measuring reflectivities within a given dynamic range, from the noise to the saturation level of its receiver. To improve this dynamic range, the wind profiler cycles through two interlaced operating modes with different pulse length. The short-pulse mode should be less prone to saturation because of its reduced sensitivity, but surprisingly, it was still found to saturate. Then, while this issue does not affect previous work such as the retrieval of the top of the boundary layer height (Chandra et al. 2010), which focused on Bragg returns (weak reflectivities typically less than 30 dBZ; Ralph 1995), a thorough setup and postprocessing are mandatory in the presence of strong signal because of precipitation.

This paper presents a rigorous quality control and processing of the wind profiler measurements aimed at providing a calibrated Rayleigh reflectivity reference and dealiased mean Doppler velocities merging the measurements of the two modes. In section 2, the wind profiler data are presented with specific highlights on the saturation and on an anomalous variability of the noise level. Then, the following section describes the different steps of the postprocessing: new estimation of noise floor (section 3a), absolute calibration using collocated disdrometer measurements (section 3b), and merging of reflectivities and Doppler velocities of the two modes (section 3c). Section 4 presents the validation of this postprocessing by comparison with a high-quality centimeter-wavelength profiler deployed at the ARM SGP site during the Midlatitude Continental Convective Clouds Experiment (MC3E). Finally, section 5 shows how these updated wind profiler measurements can be used in a multiwavelengths framework for rain or brightband studies, and conclusions and perspectives are given in section 6.

2. Profiler data

Wind profilers are key instruments of ARM and they have been deployed at each ARM site since the beginning of the program. They operate at 915 MHz (33 cm) with a 9° beamwidth antenna at 3 dB and cycle through five beam directions (south, north, east, west, and vertical) with a dwell time of 30–45 s to determine the radial components from a single pointing direction. Then, the wind measurements in each direction are averaged over periods of 60 min for the production of consensus files. This configuration is optimal for wind measurements. However, because of the long dwell time, each sequence last about 5 min. Furthermore, the maximum range is limited to 3 or 5 km and the top of the troposphere cannot be sampled. These reasons may explain why the long-term dataset of ARM wind profilers has been greatly underutilized by the ARM science community.

In an attempt to fully exploit the potential of these instruments, the sampling strategy of the SGP Central Facility wind profiler was reconfigured in a single vertically looking operation mode with a very short time lapse between successive measurements (see Table 1 for the specifics of the radar), optimal for the observation of precipitation (P. Kollias 2011, personal communication). Furthermore, the wind profiler has been configured to cycle every 8 s through two interlaced operating modes with staggered PRFs and different pulse lengths. The long-pulse mode (long mode) provides high-sensitivity measurements up to 15 km, with a vertical resolution of 425 m oversampled every 212.5 m. Furthermore, most of the common Doppler velocities are accurately retrieved by this mode thanks to its large Nyquist velocity (20 m s^{-1}). The short-pulse mode (short mode) provides a better vertical resolution (62.5 m) at the price of a smaller Nyquist velocity (15 m s^{-1}). While the minimum range is the same for both modes (about 320 m), the maximum range of the short mode is only about 9.3 km. These two modes are complementary—providing low sensitivity but high resolution at short range, where the returned power signal can be large, and high sensitivity but low resolution at long range, where the signal is weaker. Therefore, the saturation problem can arise at short range, in particular for the high-sensitivity long-pulse mode.

This study makes use of data acquired with such a configuration during the MC3E field campaign, which took place in April–May 2011 at the SGP facility as part of a joint experiment between the DOE ARM and the National Aeronautics and Space Administration (NASA) Global Precipitation Measurement mission ground validation. The suite of instruments involved in this experiment provides an unprecedented opportunity for the characterization of clouds and precipitation. Several instruments suited for precipitation measurements were deployed in close proximity to the wind profiler. Specifically, for this study, a two-dimensional video disdrometer (2DVD) provides rain size distribution characterization at the ground, while a high-quality S-band profiler (Gage et al. 2002; Williams et al. 2007) can be used to evaluate the performances of the wind profiler data after the postprocessing proposed in this work.

The entire wind profiler dataset recorded during MC3E has been analyzed, but for simplicity, a single rain event will serve as illustration throughout the paper. The chosen event (called the MC3E dream scenario) is a mesoscale convective system that moved over the SGP facility on 20 May. The time–height plot of the signal-to-noise ratio (SNR) as recorded by the real-time processing software (Vaisala LapXM) of the wind profiler during this squall line is shown in the top row of Fig. 1.

TABLE 1. Specifics for the two operational modes of the ARM profiler in the new sampling strategy.

Parameters	Short mode	Long mode
Pulse width (ns)	417	2833
Range resolution (m)	62.5	425
Sampling resolution (m)	125	212.5
Height of first gate (m)	320	320
Max height sampled (km)	9.3	15.3
No. of range gates	75	75
Interpulse period (μs)	100	120
No. of coherent integrations	56	34
Nyquist velocity (m s^{-1})	14.7	20.07
Spectral resolution (m s^{-1})	0.23	0.31
No. of points in spectra	128	128
No. of spectral average	4	4
Dwell time (s)	3	3
No. of profiles (min^{-1})	10	10
Dynamic range (dB)	80	80

As expected, the SNR of the long-mode SNR_{LM} (top-left panel) is greater than that of the short-mode SNR_{SM} (top-right panel), since the long mode has a better sensitivity. Obviously, the two modes show the same features, with three apparent portions of the rain event: 1) some convection embedded in stratiform precipitation as revealed by the bright band visible at about 3.5-km height between 0600 and 1000 UTC; 2) a deep convective cell around 1030 UTC; and 3) stratiform rain with a well-defined bright band from 1100 to 1600 UTC. Because of its lower sensitivity, the short-mode signal becomes indiscernible from noise above 6-km height. Hence, at higher altitudes, the precipitating cloud is only detected by the long mode. Another visible feature is that the SNRs in the first two range gates of the long mode seem to be slightly weaker than above, in particular in the convective cell period. While slight evaporation near the ground can be responsible of a decrease of SNR with decreasing height, it cannot explain such a large decrease, sometimes exceeding 5 dB, in a few hundred meters. On the contrary, this can be due to saturation of the receiver. This assumption seems to be confirmed by the fact that this decrease is not visible in short-mode measurements, except during the convective cell.

a. Saturation issue

Two-dimensional frequency distributions of reflectivity (2DFD) (Gage et al. 1999; Williams et al. 2000) are the perfect graphical tools to make the saturation issue evident. Top panels of Fig. 2 show the 2DFDs of SNR_{LM} (top-left panel) and SNR_{SM} (top-right panel) during the squall-line event (same data as shown in the top row of Fig. 1). Using this representation, the grayscale

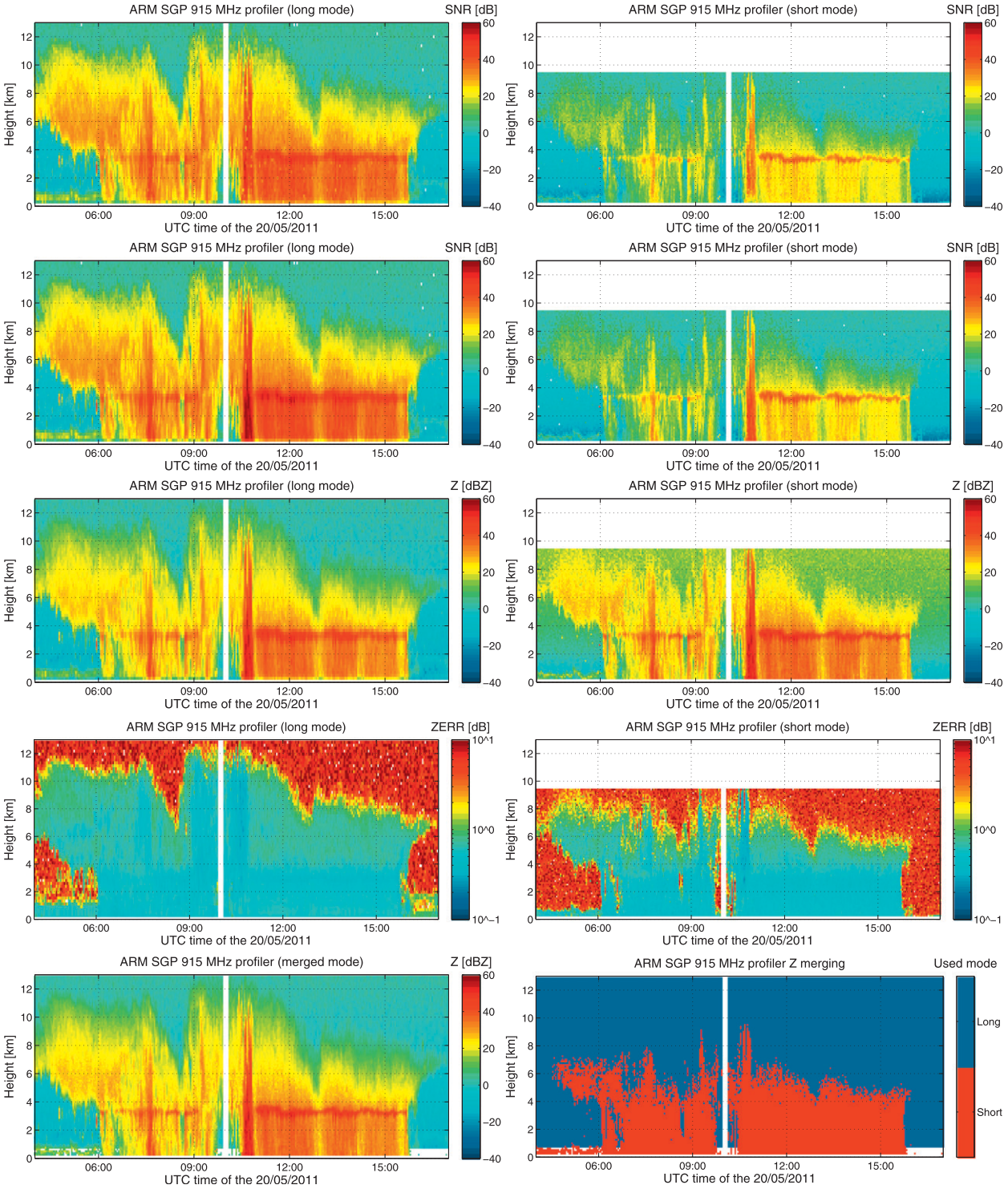

FIG. 1. Wind profiler data after each step of the signal processing for the (left) long mode and (right) short mode: SNR (level 0) in first row; SNR (level 1) in second row; calibrated reflectivity and its associated standard deviation in third and fourth rows, respectively; and final merged reflectivity in last row, next to a flag parameter showing the source of merged reflectivity.

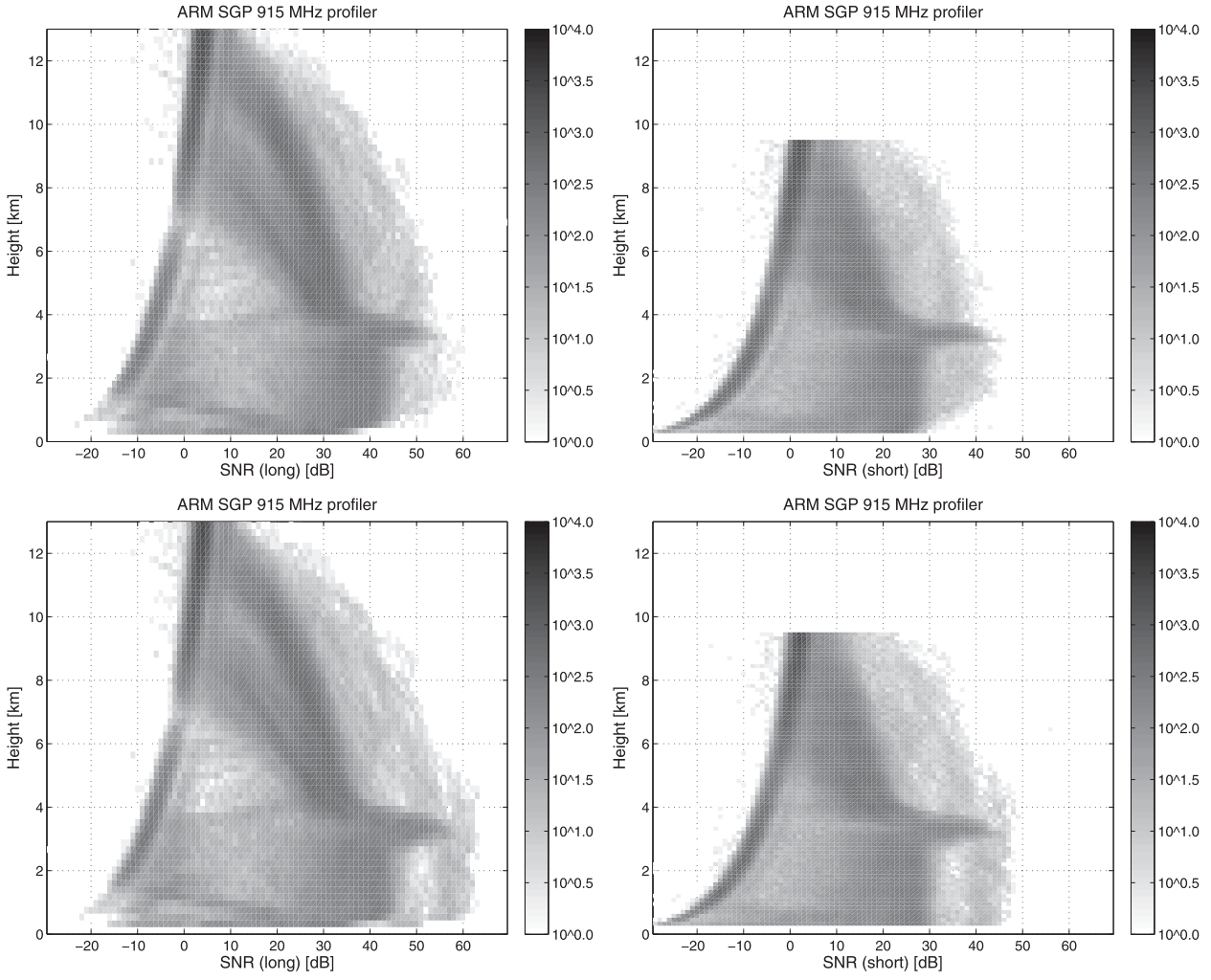

FIG. 2. 2DFDs of raw SNR measured by the wind profiler for (left) long and (right) short modes.

shows the number of occurrences of data points for the corresponding SNR value and height. Precipitation features are easily recognized, with the majority of data points showing a profile almost constant until the brightband height is reached at about 3.5 km, and a slightly decreasing signal with increasing height above, a typical feature of ice-phase precipitation above the bright band. The distributions are bounded between two threshold values that are increasing with altitude proportionally to the square of the height. The lower limit is the noise level with a high number of occurrences. The higher limit corresponds to saturation of the receiver (radar front end or analog-to-digital converter saturation).

Since the wind profiler is not using the same pulse lengths, we do not expect the same level of saturation as observed in Gage et al. (1999). It appears that this level is reached for an SNR of around 50 dB at 1 km for the highly sensitive long mode. The short mode was partly devised to avoid such saturation, and it is a surprising result that the short mode seems also to suffer from receiver saturation. In the following, it will be shown that, in this present configuration, this is not the saturation of the receiver that is capping the SNR of both modes near the ground.

b. Noise variability issue

Before any Doppler moment can be computed, the mean noise power must be removed. Noise is known to be slightly variable in time. In the real-time processing software of the wind profiler, its level is therefore estimated from each spectrum using the classical technique developed by Hildebrand and Sekhon (1974) based on the fact that the noise has a white spectrum. This technique is widely used and has proved to work well in a wide variety of situations. But, as shown by the time–height

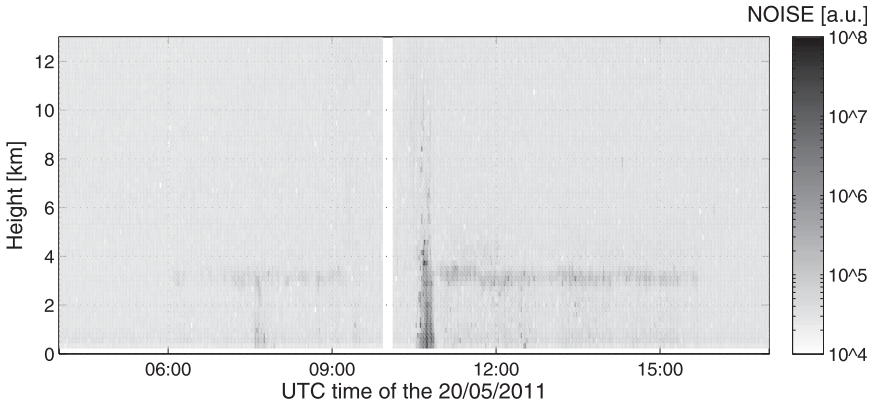

FIG. 3. Time–height plot of the noise determined by the routine processing of the wind profiler for long mode.

plot of the noise for long mode (Fig. 3), the wind profiler noise level is much more variable than expected with variability spanning more than two orders of magnitude. This is particularly the case around the bright band and in heavy precipitation corresponding to the convective cell region. Figure 4 shows an example of a precipitation spectrum measured during this convective cell. It is associated with a high level of noise compared to the noise spectrum of a clear-air gate measured at 15 km during the same dwell. Generally, the noise level can be overestimated when the precipitation spectrum width is so large that it extends over a large part of the Nyquist interval, thus reducing the number of spectral points that contain just noise. This problem is even amplified by the large beamwidth of the wind profiler (9°), which can significantly widen the measured spectrum in presence of important turbulence and wind shear. But for the wind profiler, this mechanism cannot explain this variability, since even a wide precipitation spectrum of 5 m s^{-1} such as the one in Fig. 4 is narrow compared to the Nyquist interval of the wind profiler. In the present case, the noise floor seems to be really higher because of the incoherent signal return from hydrometeors because of potential transmitter pulse phase noise.

3. Postprocessing of wind profiler data

To circumvent and mitigate the previous issues, postprocessing has been designed for profiler data along the following guidelines, illustrated in Fig. 5, where the initial SNR data are defined as SNR_{LM} and SNR_{SM} (level 0). First, a method for providing an improved estimate of the noise level is proposed, which leads to new SNR_{LM} and SNR_{SM} (level 1). By comparison with collocated disdrometer measurements, the two modes of SNR are then calibrated to provide reflectivity data Z_{LM} and Z_{SM}. Finally, they are merged into a single set of reflectivity data Z with a high dynamic range. Similarly, mean Doppler velocities are computed from the new signal estimates and are then dealiased and merged. Following the algorithm logical thread, Fig. 1 presents the wind profiler data at each step, for the already mentioned 20 May 2011 precipitation case.

a. Determination of noise level from clear-air echoes

The signal dwell of both modes is very short, so that the noise level computed at different gates of the same profile should not vary significantly. Hence, the proposed solution is to use the noise estimations made at

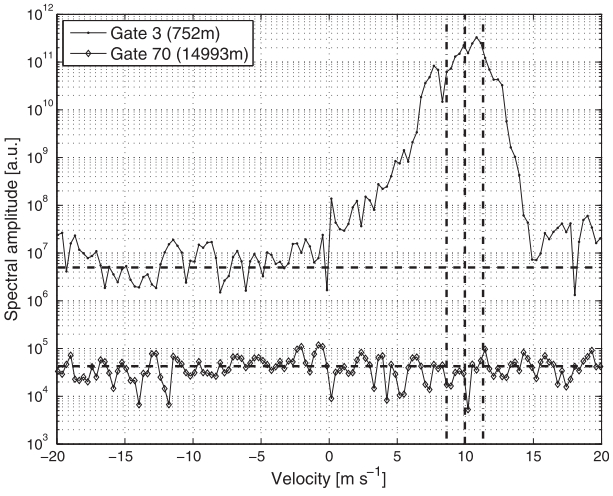

FIG. 4. Instantaneous rain and noise spectra measured during the convective cell at 1044:57 UTC at 0.75- and 15-km height, respectively. Horizontal dashed lines correspond to the noise level estimated using the routine processing, and vertical dashed and dotted–dashed lines show the mean Doppler velocity and the spectral width of the rain spectrum, respectively.

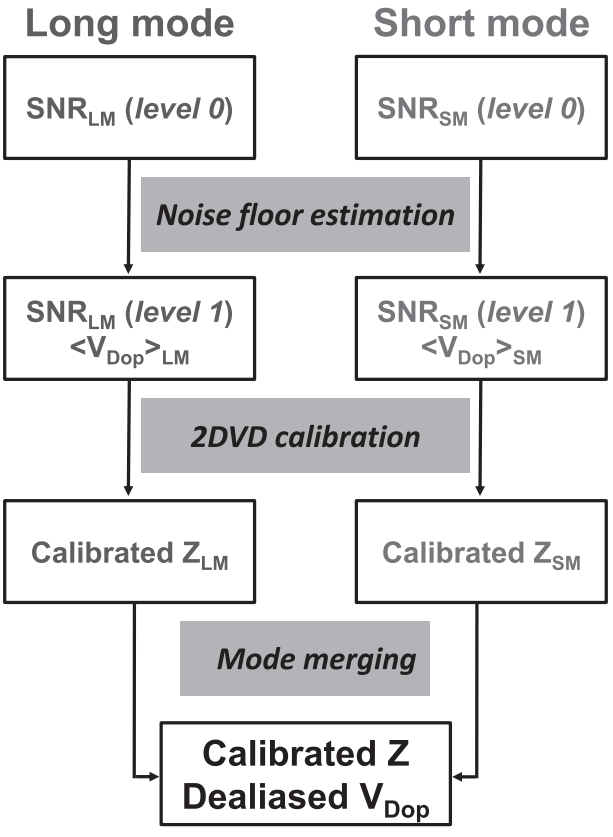

FIG. 5. Flowchart of the wind profiler signal postprocessing.

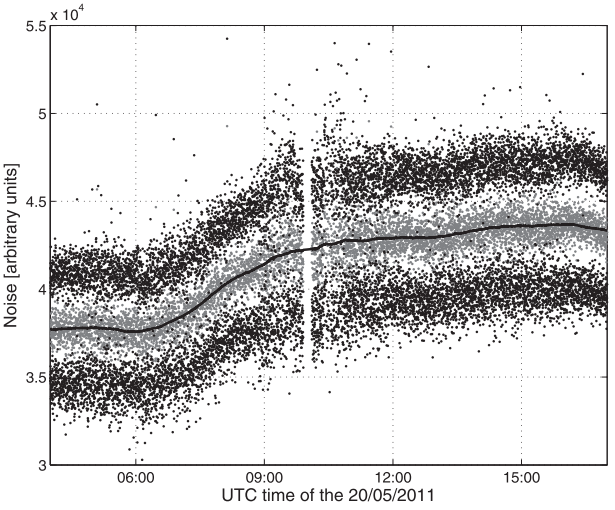

FIG. 6. Noise variability as retrieved from long-mode clear-air echoes for the 20 May 2011 event shown in Fig. 3 (see text for details).

hydrometeor- and Bragg-free gates to determine a mean noise level for the whole profile. A similar procedure is followed to retrieve the noise floor variability of National Oceanic and Atmospheric Administration (NOAA) profilers (C. R. Williams et al. 2012, personal communication) and of the 94-GHz *CloudSat* radar (Tanelli et al. 2008). The hydrometeor- and Bragg-free gates are identified by using a combination of thresholds on the spectral width and the SNR as follows: while a maximum spectral width of 0.5 m s^{-1} is used for both modes, a maximum level 0 SNR of −10 and −12 dB has been selected for the short and long modes, respectively. A mean noise estimation is then obtained for each profile by averaging the clear-air gate returns. Figure 6 shows these mean noise estimates (gray dots) and the associated standard deviation (black dots at mean noise ± standard deviation) for the long-mode measurements during the squall line presented in Fig. 1. A similar figure can be obtained for the short mode.

In convective situations meteorological targets may extend over the whole troposphere and hence meteorological spectra can be measured over the majority of gates and even over the full profile for the short mode (which extends up to 9.5 km only). To avoid erroneous noise floor determinations for these cases, the noise estimate is kept only when more than 10 clear-air gates are available and if the corresponding standard deviation is not too large. Furthermore, a running average (black line in Fig. 6) with a time window of 60 min is performed on the mean noise values. This permits filling in of the missing estimates (e.g., around 1000 UTC in Fig. 6) while keeping the natural variability of the noise level, which changes by ±30% around its mean level during the whole MC3E campaign. Note that at this frequency, the emissions from gases and precipitation are believed to play a negligible role. Hence, instead of being external, the major source of the noise variability seems to be internal, which guarantees a smooth temporal variability and justifies the use of a running average of 60 min.

The overestimation of the noise level leads naturally to an underestimation of the SNR and potential errors in Doppler velocity and spectral width. These three parameters are computed again from the raw spectra and the new noise estimation. The second row of Fig. 1 shows the resulting SNR$_{LM}$ and SNR$_{SM}$ (level 1) with the new noise estimation. It is visible that the major changes happen mostly in high SNR parts, near the bright band and in cores of heavy precipitation. For a better appreciation of this effect, a zoom of the 1000–1100 UTC period for the long mode is depicted in Fig. 7 with SNR$_{LM}$ (level 0) (top panel) and SNR$_{SM}$ (level 1) (bottom panel). This demonstrates that the underestimation can be very large, with differences as high as 20 dB. Furthermore, some precipitation features near the consecutive cells visible between 1035 and 1040 UTC

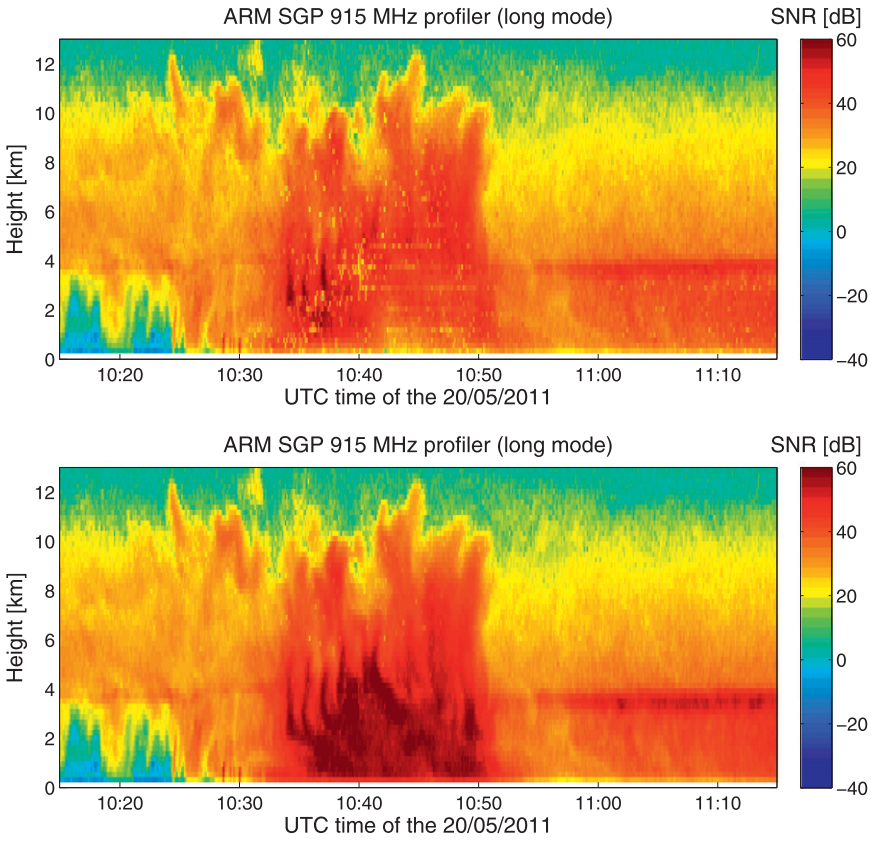

FIG. 7. SNR of the long mode with the (top) previous and (bottom) new noise estimates.

and between 2 and 6 km are totally missed in the SNR_{LM} (level 0). On the contrary, it is visible that there is no effect on the low SNR parts. Particularly, the areas of Bragg scattering only (e.g., before 0600 UTC and below 1 km on Fig. 1), which were used by Chandra et al. (2010), are not affected. Similarly, estimations of mean Doppler velocity and spectral width from the routine processing were correct for low SNRs, while in the case of strong SNRs, the noise is several orders of magnitude lower than the hydrometeors' signal. Therefore, overall, the overestimation of the noise level had almost no effect on the mean Doppler velocity and spectral width, and these parameters were not influenced by the modification of the noise level on the spectrum of Fig. 4. Given the previous use of the wind profiler data, this explains why this issue was not identified and investigated before in the ARM wind profiler datasets.

In the convective cell, the decrease with decreasing height of the short-mode SNR at short ranges, which was diagnosed as a saturation effect, is no longer visible in the level 1 data (Fig. 1, second row, right panel). This means that the saturation effect seen in the top panels of Fig. 2 and apparently due to radar front end or analog-to-digital converter saturation is actually due to erroneous noise estimation. The update of the 2DFD of both modes with level 1 SNRs (bottom panels in Fig. 2) reveals that saturation is clearly not visible anymore. For the long mode, the whole measurements in the first two range gates seem still to be shifted by approximately −10 dB (also visible in the second row of Fig. 1 in the left panel). Since the measurements of the wind profiler come from an average of several pulses, whose backscattered power is distributed exponentially around the mean (Zrnić 1975), the effect of saturation can be perceived below its true level. But simple simulations indicate that it cannot be perceived more than 7 dB below this level. The underestimation of SNR_{LM} in the first two range gates can indeed be explained by a receiver saturation effect due to a delayed switching on of the receiving mode. As a consequence, the corresponding data are underestimated and should not be used for further calibration and merging.

b. *Calibration*

Absolute radar calibration is an important but difficult task. While direct calibration of scanning radars is challenging but possible by tracking a known target, it is impractical for profiling radars. One solution proposed

by Gage et al. (2000) and further developed by Williams et al. (2005) is to compare the signal measured by the wind profiler in the lowest range gate with the reflectivity computed from the drop size distribution (DSD) measured by a collocated disdrometer. This comparison is made in decibel units in order to obtain a normally distributed probability density function (PDF) and to compute a statistically significant standard deviation and confidence interval. Then, the obtained mean difference is used to calibrate the wind profiler by simply adding it to the SNR (in dB). Furthermore, if enough data are available, this mean difference can be computed by intervals of disdrometer reflectivities to evaluate and interpret the behavior of this calibration constant as a function of the reflectivity.

Two major factors can affect the accuracy of the calibration when adopting this method: mismatch in sampling volume size and height/time difference between the samples. Obviously, these effects increase with the height at which the wind profiler measurements are made and the lowest possible range gates should be taken. For the long mode, since the first two range gates have been proved to underestimate the SNR, the lowest reliable measurements are at a mean height of about 750 m. On the contrary, for the short mode, the first range gate is at 325 m, which makes this mode better suited for this calibration method. Similarly, Williams et al. (2005) obtained good results with wind profiler measurements centered at a height of 308 m. Therefore, the 2DVD measurements can be used to compute the radar constant for the short mode. Since the two modes have different pulse length and number of coherent integrations, this constant is not relevant for the long mode and the long mode will then be calibrated by intercomparison with the short mode.

1) SHORT-MODE CALIBRATION

The 2DVD (Kruger and Krajewski 2002) detects each drop passing through its measuring area formed by the section of two orthogonal light sheets. This sampling area being quite small (about 1 m^2), an integration time of 1 min is the minimum required to provide statistically significant samples. The obtained DSD allows for computation of the 2DVD Rayleigh reflectivity Z_{DVD} with a 1-min time resolution. The SNR_{SM} (level 1) from the lowest range gate of the wind profiler is averaged in time to correspond to the 1-min resolution of the disdrometer. At this resolution, the time needed for the drops measured by the wind profiler at 300-m height to reach the ground is comparable with the 2DVD time resolution and can be ignored. Furthermore, since the reflectivity is proportional to the sixth moment of the drop size distribution, the evaporation of small drops during their fall to the ground should not affect the comparison.

Following Williams et al. (2005), the PDF of the difference (in dB) between Z_{DVD} and wind profiler SNR_{SM} allows the computation of the mean difference and standard deviation. Furthermore, the differences and their confidence intervals at the 95% level are computed for disdrometer reflectivity intervals. The results are plotted in Fig. 8 with the difference $Z_{DVD} - SNR_{SM}$ as function of Z_{DVD}. The y axis is centered around the mean difference between the two instruments at 10 dB (horizontal lines), while the dotted–dashed lines show the standard deviation of 2.6 dB. This nonnegligible standard deviation is similar to the one obtained by Williams et al. (2005) and can be explained by the different operating principles of the two instruments and their difference in sampling volume and height.

The confidence level shown in Fig. 8 is good for the estimates ranging between 20 and 40 dBZ; it becomes poor outside of this range because of the reduced sample size. The behavior of the difference between the two instruments is similar to the one reported by Gage et al. (2002) when calibrating a Next Generation Weather Radar (NEXRAD) S-band radar with a 915-MHz wind profiler. The estimates are quite stable from around 25 to 45 dBZ, while they sharply decrease for lower reflectivities, indicating that the wind profiler reflectivity becomes greater than the 2DVD one, a clear signature of Bragg scattering detected by the wind profiler. Similarly, for the calibration of their 2.8-GHz profiler, Williams et al. (2005) used a lower threshold of 10 dBZ in order to ensure that only precipitation was measured. Indeed, the lower the radar frequency, the greater the sensitivity to Bragg scattering. Figure 1 of Ralph (1995) shows that, at 915 MHz, values of Bragg scattering as strong as 30 dBZ can even occur, although rarely. In the MC3E dataset, it seems sufficient to keep reflectivities higher than 25 dBZ to compute the final calibration constant. As a result the gray part in Fig. 8 (i.e., 2DVD reflectivities lower than 25 dBZ and greater than 45 dBZ) is discarded. The remaining data lead to the calibration constant of 10 dB, which can then be used to compute the short-mode-calibrated reflectivity Z_{SM}.

2) LONG-MODE CALIBRATION

The long-mode calibration can be performed by an intercomparison between both modes' SNRs (level 1). A larger dataset is available for this comparison, since the 8-s time resolution of the wind profiler can be used. Furthermore, following Williams et al. (2005), who compared the 2.8- and 915-MHz profilers' measurements, all heights can be used. Then, for this comparison, SNR_{LM}

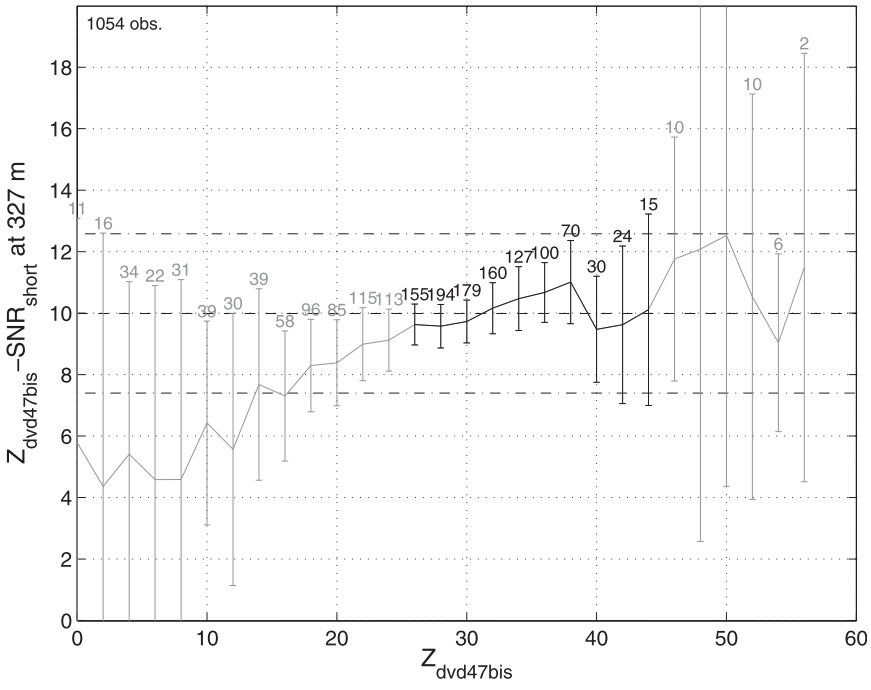

FIG. 8. Bias between Z_{DVD} and profiler SNR_{SM} (level 1) as function Z_{DVD}. Number of measurements in each bin is indicated at the top of the corresponding error bar.

(level 1) is interpolated at short-mode heights and the areas with high vertical reflectivity gradient (more than 2.5 dB between two successive range gates) are discarded to avoid interpolation artifacts (e.g., particularly acute in the bright band).

The resulting mean difference between both SNRs for height between 1 and 5 km is shown in Fig. 9 by intervals of SNR_{SM}. Similar to the intercalibration of two different profilers discussed by Williams et al. (2005), the correspondence between short and long modes is excellent

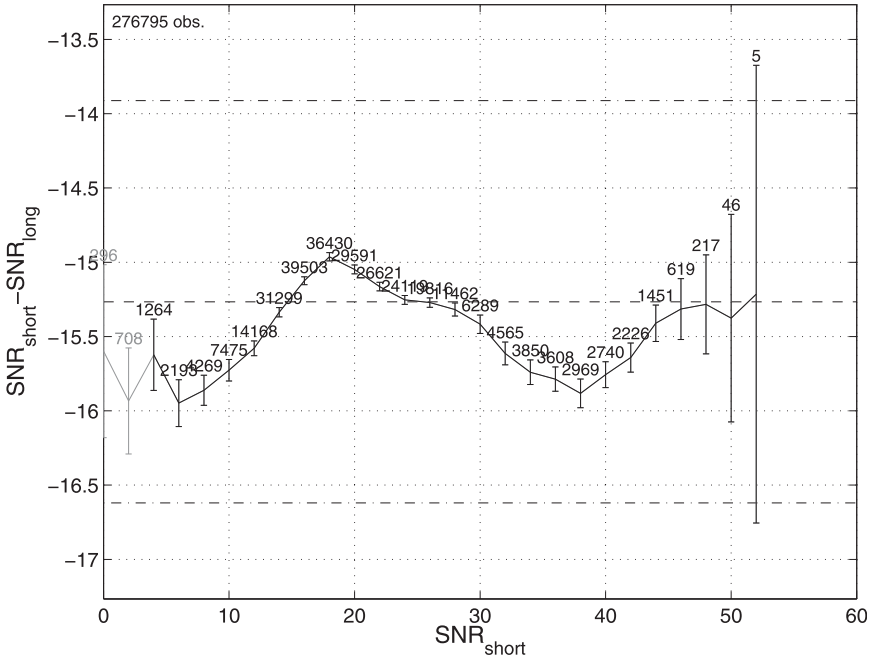

FIG. 9. As in Fig. 8, but between SNR_{SM} and SNR_{LM} (level 1) as function of SNR_{SM} (level 1).

with a global standard deviation of less than 1.5 dB and a difference varying by about 1 dB for SNR_{SM} values ranging from 5 to 55 dB. The fact that the results are slightly worse than those obtained in Williams et al. (2005) is a little surprising, since they compared reflectivities measured by two radars operating at different frequencies. But this can be explained by the fact that their radars were matched in beams and resolution, while here the two modes have a different range resolution. Besides, in the present case, since the transmitted frequency is the same for the two datasets, all types of scattering can be used to compare them, and there is no need to take a lower limit to avoid Bragg scattering.

The final difference of 15.3 dB between the two modes (see Fig. 9) is in good agreement with the value of 14.5 dB deduced from theoretical considerations, suggesting that the radar calibration constant is roughly proportional to the inverse of the square of the pulse length and of the number of coherent integrations (see values in Table 1). Finally, the long mode can be calibrated with a constant of −5.3 dB by taking into account the absolute calibration constant of the short mode determined before. The calibrated Z_{LM} and Z_{SM} are shown in the third row of Fig. 1. The reflectivities of the two modes correspond very well, while the higher levels of noise for short mode are self-evident.

c. *Merging of the modes*

The third row of Fig. 1 shows that precipitation features such as the bright band are better resolved by the short mode thanks to its higher resolution. On the other hand, Z_{SM} hits the noise level at lower heights (roughly about 6 instead of 9 km for Z_{LM}). Therefore, it is worth producing a merging of the two modes that combines the advantages of both, that is, high vertical resolution and long maximum range.

Similarly, short-mode Doppler velocities are retrieved with a better height resolution, while the larger Nyquist interval of the long mode reduces the risk of velocity aliasing. Hence, the Doppler velocities of the two modes can be combined to produce a merged Doppler velocity product with the advantages of both modes. Thanks to these merged products, the scientific community will not have to address the particularities of each sampling mode, and the use of the ARM wind profiler data will be facilitated.

1) REFLECTIVITY MERGING

An interpolation of Z_{LM} profiles at short-mode height would only provide a smoother version, that is, with fewer details, of Z_{SM} profiles. Therefore, the merged product is not computed here as the average between short- and long-mode reflectivities, but it is defined equal to either Z_{SM} as long as its quality is sufficient or Z_{LM} otherwise. One exception is that Z_{LM} at the two first range gates is never retained. The merged profiles are determined at each short-mode time step. Hence, the short-mode reflectivities are directly copied, while for the long mode the two nearest profiles are averaged and then interpolated at short-mode heights before being incorporated.

The critical parameters for the quality of the reflectivity are the SNR and spectral width following the appendix in Hogan et al. (2005). For the purpose of merging, the standard deviation of the measured reflectivity is computed for each gate and profile (fourth row of Fig. 1). The standard deviation generally ranges between about 0.3 and 0.6 dB when the SNR is higher than 0 dB; however, it increases rapidly otherwise, about 6 and 8 km in the stratiform part of the rain event for the short and long modes, respectively. When the standard deviation of the two modes is equivalent, the short mode is preferred because of its better height resolution. Hence, Z_{SM} is used in the merged product as long as its standard deviation is lower than a threshold of 0.8 dB.

The resulting merged reflectivity time evolution is plotted in Fig. 1 (fifth row, left panel) next to a flag showing the source of data (fifth row, right panel). As expected, the merged reflectivity has the high resolution of a short mode at low and medium ranges (e.g., compare the brightband thickness with the third row in Fig. 1), while some significant reflectivities are recorded at long range (up to 10 km). Besides, it is interesting to note that the maximum height at which Z_{SM} can be used is varying. While, in this example, this level is, on average, at about 5-km height, it can increase when the reflectivities are greater, as during the convective portion of the event, where it reaches 9.5 km.

2) DOPPLER VELOCITY MERGING

The profiler is operated in staggering mode with the long mode having a longer pulse repetition time (PRT), thus longer Nyquist interval, than the short mode (see Table 1). The merging of the two modes allows the reconstruction of Doppler velocities over a velocity interval larger than the long-mode Nyquist interval (Doviak and Zrnic 1993; Torres et al. 2004). At vertical incidence, Doppler velocities measured in rain are a combination of terminal fall velocity of hydrometeors and vertical wind speed; these velocities cannot generally exceed +45 and −25 m s^{-1} (with positive downward velocity). Since the Nyquist velocities of both modes are large enough, we can consider, for the sake of simplicity, that the Doppler velocities can be folded only once for each mode. This means that the maximum Doppler velocities that can be reconstructed are

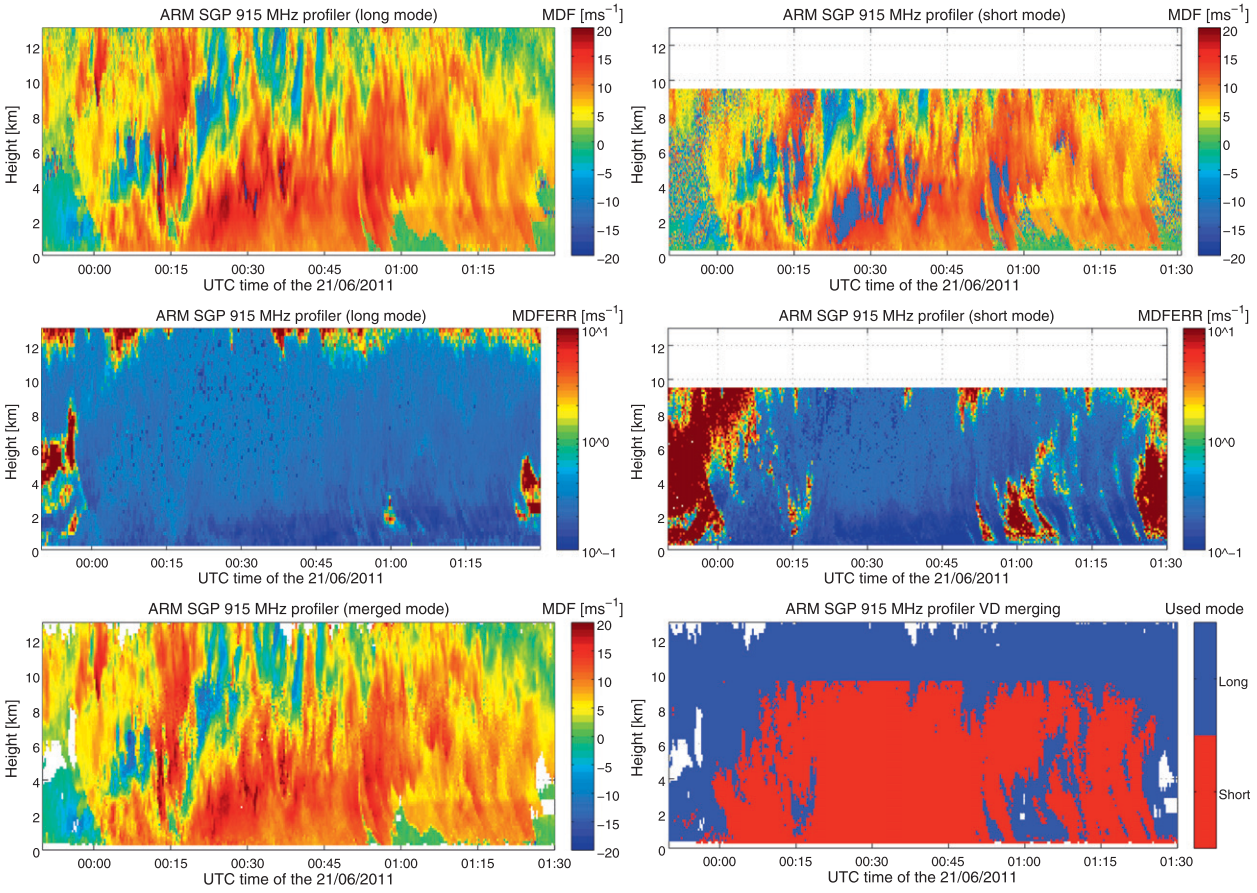

FIG. 10. Merging of the Doppler velocity of the two modes. Note that the color scale is limited between −20 and +20 m s^{-1}.

limited by 3 times the short-mode Nyquist interval, that is, ±45 m s^{-1}.

As long as aliasing is not corrected, the Doppler velocities can be neither averaged nor interpolated. Hence, the first step of the merging is the dealiasing of the Doppler velocities of both modes by comparing both space and time nearest-neighbor estimates. Among the nine pairs of Doppler velocities obtained by unfolding the initial long-mode (short-mode) velocities into the ±60 (±45) m s^{-1} intervals, the one with the most similar values is selected. But, because of the mismatch in height resolution of the two modes and/or of the rapid time variation of vertical wind during convective cases, the velocity estimates may not correspond well, thus leading to the wrong choice of dealiased velocity combination for some data points. Such outliers can be removed by vertical continuity correction applied to each profile and by imposing, when necessary, the boundary condition of $-10 > V_{\mathrm{Dop}} < 20$ m s^{-1} vertical wind near the ground.

Since Doppler velocities are now dealiased, the long-mode estimates can be interpolated at short-mode height. Finally, similar to the merged reflectivity product, the merged Doppler velocity follows the short-mode dealiased Doppler velocities when their corresponding standard deviation (computed from Doviak and Zrnic 1993) is below 0.3 m s^{-1} and the long-mode dealiased Doppler velocities otherwise.

This Doppler velocity dealiasing and merging method is illustrated in Fig. 10. Since no aliasing effect was visible in the 20 May 2011 case, data of 21 June 2011, a deep convective system showing some of the most intense vertical winds observed during MC3E, were chosen for this illustration. The first row in Fig. 10 shows the initial Doppler velocities of both modes with evident aliasing for the short mode at various time steps and heights, but also visible for the long mode at 4 km around 0013 and 0030 UTC. The second row shows the corresponding standard deviation, primarily ranging between 0.1 and 0.4 m s^{-1} but increasing rapidly for SNR (not shown) below 5 dB. Finally, like for the merged reflectivity product, the resulting dealiased and merged Doppler velocity time evolution is plotted in the third row (left panel) next to a flag showing the source of data (right

panel). To validate this processing, there was unfortunately no other radar using a larger Nyquist velocity collocated to the wind profiler on this day. However, from Fig. 10, it is qualitatively clear that it is providing well-dealiased Doppler velocities.

4. Validation

In this section, the accuracy of the wind profiler data postprocessing is verified by comparing the resulting merged reflectivity with the reflectivity measured by the NOAA S-band profiler collocated with the wind profiler during the MC3E campaign.

To assess the quality of the wind profiler measurements against the S-band profiler, it must be ensured that their respective absolute calibrations are consistent and do not provoke any additional discrepancies. Two factors can affect this calibration: differences between the instruments used as calibration reference and a drift with time of the power measured by one or both profilers.

Because of the inhomogeneity of precipitation and of the small sampling area of in situ instruments, disagreements are usually observed between collocated disdrometers, in particular during heavy rainfall events (Krajewski et al. 2006). All types of disdrometer have some instrumental limitations. For example, Joss–Waldvogel disdrometers detect drops within a limited range of sizes, at small diameters because of a dead time problem and at large diameters because of its maximum detectable size (Tokay et al. 2002). Particle Size and Velocity (PARSIVEL) disdrometers often report a high number of smaller drops probably because of some background noise, while 2DVDs measure distorted velocities because of the wind effect due to their bulky structure (Krajewski et al. 2006). Then, in order to remove any effect due to the choice of the disdrometer in the comparison of profiler measurements, they must be calibrated using the same disdrometer. The S-band profiler, initially calibrated with a PARSIVEL deployed by NOAA, was calibrated again with the 2DVD used for the wind profiler in section 3b. The choice of the disdrometer does not change the overall results. The small MC3E dataset suggests that the 2DVD data are in better agreement with profilers, but a more comprehensive comparison should be performed on a larger dataset in order to draw general conclusions on the best disdrometer to use.

In section 3b, the calibration of the wind profiler was done on the largest data sample—that is, merging the whole MC3E dataset—in order to obtain the smallest standard deviation as possible. However, it is known that the calibration of a radar can suffer variations

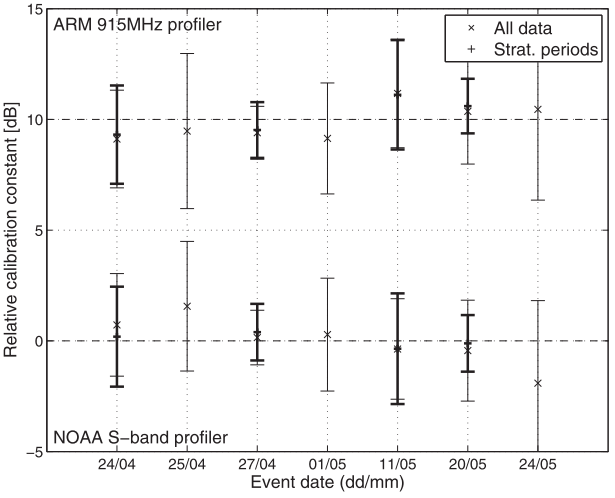

FIG. 11. Variability of event-based calibration constants of NOAA S-band profiler and wind profiler relative to the corresponding climatological ones.

because of the drift of its electronics components in time or with changes in thermodynamic conditions such as humidity and temperature. This calibration drift was assessed for both profilers by applying the calibration method described in section 3b on an event-by-event basis for seven rain events of the MC3E dataset. The corresponding calibration constants of both profilers are presented in Fig. 11. The calibration constants of the wind profiler have been shifted by 10 dB in order to improve readability. Two calibration methods have been tested: the first one using all available data with results represented by cross marks and thin lines and the second one using only manually selected stratiform periods with horizontal dash marks and bold lines. The latter method was applied on four of the events only, since a stratiform period is necessary for its application. The extent of vertical lines represents the standard deviation of the PDF of the difference between the 2DVD and the profilers. While the short convective events show a larger standard deviation, the stratiform events are associated with a smaller standard deviation, as it can be expected since the type of rain is less variable. But, the selection of stratiform data when available does not generally improve the standard deviation significantly. Finally, the calibrations of the profilers show a trend with a similar dynamic of about 1.5 dB but not necessarily in phase.

Considering this calibration drift, it can be questioned if the merging of the data from rain events separated by several days really improves the accuracy of calibration. To answer this question, the data of both profilers resulting from both calibration methods, that is, event based or climatological, were merged and compared.

The resulting PDFs of the difference between the profilers' reflectivities larger than 20 dBZ and in the first 600 m are presented in Fig. 12. As can be expected, the global difference between the data of profilers is near 0 dB for both calibration methods, since the same reference instrument was used. The small standard deviation shows that the data of the profilers are in well agreement, considering their mismatched beamwidths and height resolutions. Finally, the standard deviation associated with the event-based calibration is slightly smaller, since the calibration drift is continuously corrected.

From a calibration point of view, these results suggest that the event-based calibration should be performed as long as the length of the event is sufficient to compute a statistically significant comparison with the disdrometer. The MC3E dataset suggests that for a single event, 45 min of rain with disdrometer reflectivity larger than 20 dBZ are required for the stabilization of the calibration constant with an accuracy of 0.5 dB. The seven rain events presented in Fig. 11 fulfill this condition.

Finally, the event-based reflectivity difference is plotted in Fig. 13. This difference is well centered around 0 dB for S-band reflectivities greater than 20 dBZ. Below 20 dBZ, it becomes more negative for decreasing reflectivities because Bragg scattering becomes the dominant scattering process, and the equivalent Bragg scattering

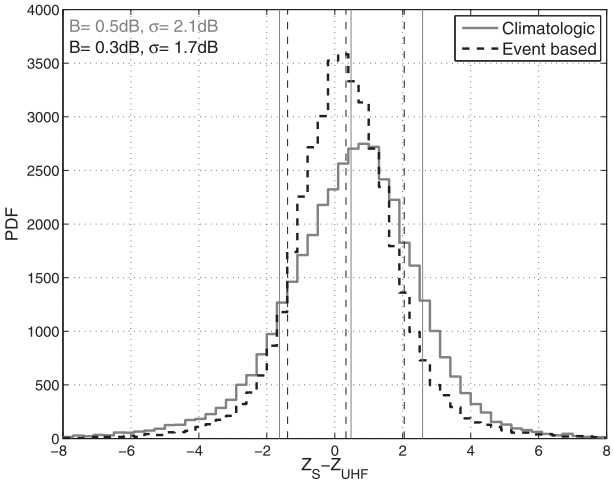

FIG. 12. PDFs of the difference between NOAA S-band profiler and wind profiler reflectivities, both calibrated on a climatological or event-by-event basis.

reflectivity is greater for the profiler with the longer wavelength (Gage et al. 1999). Between 20 and 40 dBZ, the bias is very close to zero, with a very good confidence interval of less than 1 dB. Given the mismatch between the profiler beams, these results confirm the relevance of the postprocessing of the wind profiler data proposed in section 3. The larger confidence intervals for reflectivities above 40 dBZ and corresponding to

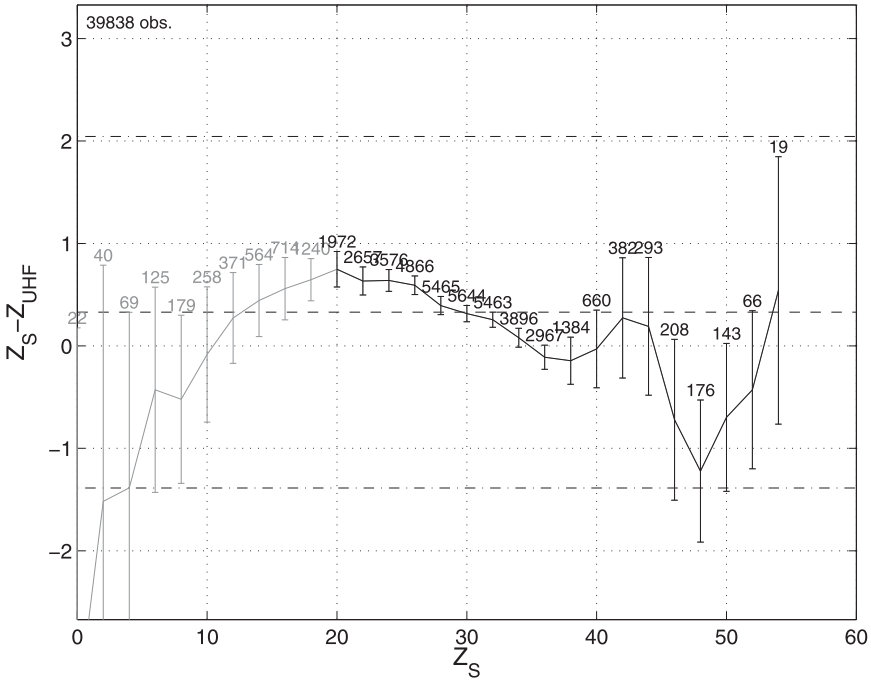

FIG. 13. Bias between NOAA S-band and wind profiler reflectivities as function of S-band profiler reflectivity. Number of measurements in each bin is indicated at the top of the corresponding error bar.

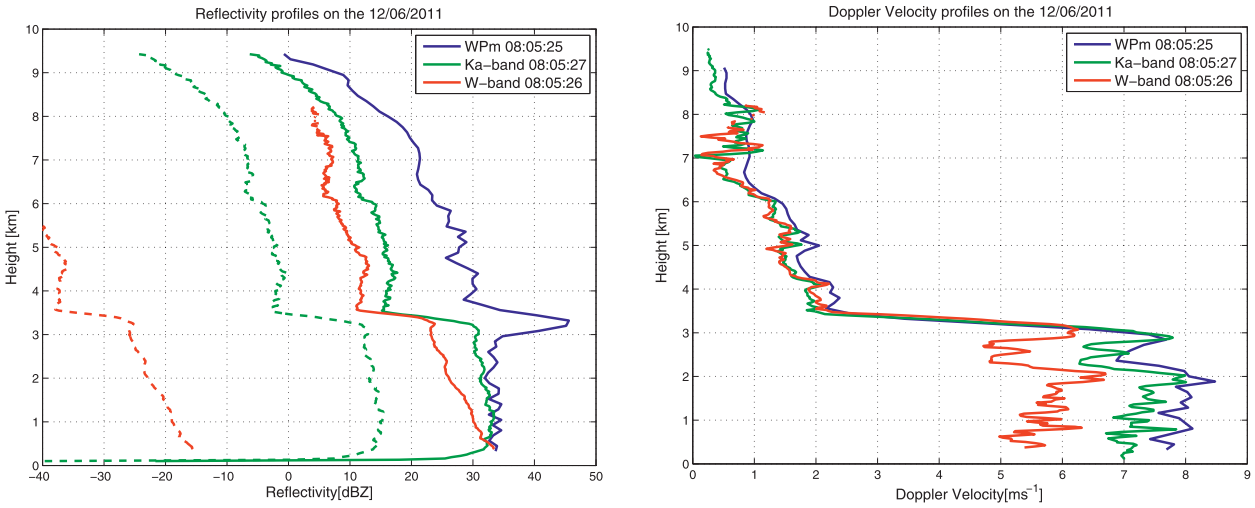

FIG. 14. (left) Reflectivity and (right) Doppler velocity profiles measured simultaneously by the ARM wind profiler and cloud radars at SGP.

convective rain are certainly attributable to this same beam mismatch.

5. Multiwavelengths studies

Numerous recent studies have shown that a combination of radars at different wavelengths can bring many benefits, taking advantage of the wavelength dependency of scattering properties in the Mie regime. Indeed, when the size of the scattering particle is similar to the wavelength, the scattering properties start to oscillate, resulting, on average, in a smaller backscattered radiation with decreasing wavelength compared to Rayleigh scattering. Figure 14 shows a nice example of a single profile measured simultaneously by the wind profiler and ARM Ka- and W-band cloud radars at the ARM SGP site on 12 June 2011. In this section, some examples of possible multiwavelength studies will be given, with a particular emphasis on the benefit brought by the postprocessing and calibration of the wind profiler presented in this paper.

a. Estimation of radome attenuation

The wind profiler reflectivity profile shown in Fig. 14 (blue line in the left panel) is typical of stratiform precipitation with a well-defined bright band at about 3.3-km height. The raw reflectivity profile of the cloud radars is represented by the dashed lines. The Ka-band receiver is clearly saturated up to a level of about 500 m. Apart from the differences in the sampling volume, the fact that the cloud radars' reflectivity at 1 km (hence, above the saturation level) is greatly lower than the wind profiler reflectivity is due to a combination of several factors: the Mie effects for large drops in the scattering volume, the attenuation of microwave radiation in the layer below, miscalibration of the cloud radars, and radome attenuation. Mie effects and rain attenuation can be estimated using the collocated disdrometer data, assuming that the rain layer below is homogeneous. Finally, radome attenuation can be estimated only if the cloud radars are previously calibrated.

b. Rain-rate retrieval

To clearly observe the differential effects in the rain layer, the cloud radars' reflectivities can be matched to the wind profiler reflectivities at the level where the receiver is not saturated any more (continuous lines on Fig. 14): the clouds radar reflectivities decrease with height up to the brightband level because of rain attenuation. Then, this rain attenuation at millimeter wavelengths is a significant parameter that can be used to retrieve properties of precipitation. For example, at Ka band, attenuation is closely linked to rain rate. But, the Mie effects can also vary with height if the DSD profile is not perfectly constant with height. The signature of these Mie effects is evident in the Doppler velocities profiles (right panel). Since Doppler velocities are unaffected by miscalibration issues or attenuation, the difference between Doppler velocities occurs because at millimeter wavelength, large drops are associated with a reduced reflectivity compared to medium-size drops; hence, the cloud radar reflectivities are dominated by smaller drops that fall at lower velocities. Finally, while absolute calibration is not necessary for attenuation-based retrievals, it is an essential asset if a full DSD retrieval has to be performed.

c. Melting-layer attenuation

Attenuation produced by melting particles is known to be substantial at cloud radar wavelengths but difficult to estimate because of uncertainties in their microphysical and scattering properties. Yet, melting-layer attenuation is a key parameter for the attenuation-based retrieval of rainfall from airborne or satellite-borne cloud radars. By matching reflectivities just below the melting level, it is possible to retrieve the brightband attenuation at millimeter wavelengths. In Fig. 14 (left panel), the Ka- and W-band radar reflectivity features near the brightband level of the wind profiler are typical of cloud radars: the increase in reflectivity in the first part of the melting level is counterbalanced by attenuation and the resulting effect for the whole melting layer is a strong decrease in reflectivity. Above the melting level, the difference in reflectivity between the wind profiler and cloud radars is due to this brightband attenuation combined with the Mie effects and attenuation of the rain below. Then, the melting-layer attenuation can be estimated by simple differentiation from the upper part of the ice cloud, where all wavelengths are scattering in the Rayleigh regime.

6. Conclusions and future work

The recent reconfiguration of the ARM 915-MHz wind profilers with staggered PRFs and vertical incidence make them an ideal low-cost instrument for providing reflectivity and Doppler velocity profiles of precipitation with high temporal and vertical resolutions at every ARM site. This paper details the postprocessing procedure necessary to produce absolutely calibrated Rayleigh reflectivity profiles and dealiased Doppler velocities, which can serve as references for multiwavelengths retrievals in synergy with ARM cloud radars.

The first postprocessing step is the computation of an improved noise floor from clear-air estimates. This processing was proved necessary to avoid a strong overestimation of noise in heavy precipitation, which was producing underestimated SNRs, falsely interpreted as saturation. Indeed, the improved SNR variation as a function of height shows that the measurements of the wind profiler are not saturated. This is further confirmed in the second step of the postprocessing, by the very good agreement of the lowest-gate-corrected SNRs with a collocated 2DVD, which allows the computation of absolutely calibrated wind profiler reflectivities.

The wind profiler is operated using two interlaced modes with differing pulse widths and interpulse periods. The final step of the postprocessing consists of merging these modes. Indeed, thanks to the staggered PRTs and the corresponding differing Nyquist intervals, the Doppler velocities of the two modes are dealiased and then combined. Similarly, the staggered pulse widths result in reflectivity measurements with different range resolutions and sensitivities. The reflectivities of the two modes are merged in order to provide full profiles with high dynamic range and resolution.

The quality of the wind profiler data and its postprocessing are checked by comparisons with the measurements of the NOAA S-band profiler deployed nearby during the 2-month MC3E period. A very good agreement is found between both instruments with a standard deviation of 2 dB, which can even be improved to 1.7 dB when calibrating both profilers on an event-by-event basis. Therefore, as a good practice procedure for all the ARM profilers, we do recommend routinely performing reflectivity calibrations on an event-by-event basis. This obviously requires pairing each profiler instrument with a disdrometer (e.g., a 2DVD or a PARSIVEL).

In future work, ARM profiler reflectivity profiles will be used as a Rayleigh reference for comparison with attenuated reflectivities provided by collocated millimeter radars, such as the ARM Ka- and W-band zenith radars. Recently (spring of 2012), the ARM program decided to collocate wind profilers with millimeter-wavelength radar at all the sites. This setup has some potential to develop dual-frequency techniques for a wide variety of purpose. For example, in liquid phase, the comparison of vertical reflectivity gradients allows the determination of the Ka-band attenuation caused by rain, which is closely linked to rain rate and rainwater content. Furthermore, in stratiform rain, it might be possible to evaluate the Ka-band attenuation associated with the melting layer, while reflectivity comparisons in the ice phase will allow an estimation of the characteristic size of snow thanks to the Mie scattering effect at Ka band.

Acknowledgments. This work was part of the Profiling Optimal-Estimates for Rain–Cloud Efficiency Study (PERICLES) project funded by the U.K. Natural Environment Research Council. The authors thank Dr. Arunchandra Chandra for providing some of the 2DVD data and a first guess of the wind profiler calibration constant. Other data were obtained from the Atmospheric Radiation Measurement Program of the U.S. Department of Energy, and the National Oceanic and Atmospheric Administration Earth System Research Laboratory.

REFERENCES

Carter, D. A., K. S. Gage, W. L. Ecklund, W. M. Angevine, P. E. Johnston, A. C. Riddle, J. Wilson, and C. R. Williams, 1995: Developments in UHF lower tropospheric wind profiling at NOAA's Aeronomy Laboratory. *Radio Sci.,* **30,** 977–1002.

Chandra, A. S., P. Kollias, S. E. Giangrande, and S. A. Klein, 2010: Long-term observations of the convective boundary layer using insect radar returns at the SGP ARM Climate Research Facility. *J. Climate,* **23,** 5699–5714.

Doviak, R. J., and D. S. Zrnic, 1993: *Doppler Radar and Weather Observations*. 2nd ed. Academic Press, 562 pp.

Gage, K. S., C. R. Williams, W. L. Ecklund, and P. E. Johnston, 1999: Use of two profilers during MCTEX for unambiguous identification of Bragg scattering and Rayleigh scattering. *J. Atmos. Sci.,* **56,** 3679–3691.

——, ——, P. E. Johnston, W. L. Ecklund, R. Cifelli, A. Tokay, and D. A. Carter, 2000: Doppler radar profilers as calibration tools for scanning radars. *J. Appl. Meteor.,* **39,** 2209–2222.

——, ——, W. L. Clark, P. E. Johnston, and D. A. Carter, 2002: Profiler contributions to Tropical Rainfall Measuring Mission (TRMM) ground validation field campaigns. *J. Atmos. Oceanic Technol.,* **19,** 843–863.

Hildebrand, P. H., and R. S. Sekhon, 1974: Objective determination of the noise level in Doppler spectra. *J. Appl. Meteor.,* **13,** 808–811.

Hogan, R. J., N. Gaussiat, and A. J. Illingworth, 2005: Stratocumulus liquid water content from dual-wavelength radar. *J. Atmos. Oceanic Technol.,* **22,** 1207–1218.

Kollias, P., E. E. Clothiaux, M. A. Miller, B. A. Albrecht, G. L. Stephens, and T. P. Ackerman, 2007a: Millimeter-wavelength radars: New frontier in atmospheric cloud and precipitation research. *Bull. Amer. Meteor. Soc.,* **88,** 1608–1624.

——, ——, ——, E. P. Luke, K. L. Johnson, K. P. Moran, K. B. Widener, and B. A. Albrecht, 2007b: The Atmospheric Radiation Measurement Program cloud profiling radars: Second-generation sampling strategies, processing, and cloud data products. *J. Atmos. Oceanic Technol.,* **24,** 1199–1214.

Krajewski, W. F., and Coauthors, 2006: DEVEX-disdrometer evaluation experiment: Basic results and implications for hydrologic studies. *Adv. Water Resour.,* **29,** 311–325.

Kruger, A., and W. F. Krajewski, 2002: Two-dimensional video disdrometer: A description. *J. Atmos. Oceanic Technol.,* **19,** 602–617.

Matrosov, S. Y., 2005: Attenuation-based estimates of rainfall rates aloft with vertically pointing K_a-band radars. *J. Atmos. Oceanic Technol.,* **22,** 43–54.

——, 2010: Synergetic use of millimeter- and centimeter-wavelength radars for retrievals of cloud and rainfall parameters. *Atmos. Chem. Phys.,* **10,** 3321–3331.

——, P. T. May, and M. D. Shupe, 2006: Rainfall profiling using Atmospheric Radiation Measurement Program vertically pointing 8-mm wavelength radars. *J. Atmos. Oceanic Technol.,* **23,** 1478–1491.

Ralph, F. M., 1995: Using radar-measured radial vertical velocities to distinguish precipitation scattering from clear-air scattering. *J. Atmos. Oceanic Technol.,* **12,** 257–267.

Stokes, G. M., and S. E. Schwartz, 1994: The Atmospheric Radiation Measurement (ARM) Program: Programmatic background and design of the Cloud and Radiation Test Bed. *Bull. Amer. Meteor. Soc.,* **75,** 1201–1222.

Tanelli, S., S. L. Durden, E. Im, K. S. Pak, D. G. Reinke, P. Partain, J. M. Haynes, and R. T. Marchand, 2008: CloudSat's cloud profiling radar after two years in orbit: Performance, calibration, and processing. *IEEE Trans. Geosci. Remote Sens.,* **46,** 3560–3573.

Tokay, A., A. Kruger, W. F. Krajewski, P. A. Kucera, and A. J. P. Filho, 2002: Measurements of drop size distribution in the southwestern Amazon basin. *J. Geophys. Res.,* **107,** 8052, doi:10.1029/2001JD000355.

Torres, S. M., Y. F. Dubel, and D. S. Zrnić, 2004: Design, implementation, and demonstration of a staggered PRT algorithm for the WSR-88D. *J. Atmos. Oceanic Technol.,* **21,** 1389–1399.

Williams, C. R., W. L. Ecklund, P. E. Johnston, and K. S. Gage, 2000: Cluster analysis techniques to separate air motion and hydrometeors in vertical incident profiler observations. *J. Atmos. Oceanic Technol.,* **17,** 949–962.

——, K. S. Gage, W. Clark, and P. Kucera, 2005: Monitoring the reflectivity calibration of a scanning radar using a profiling radar and a disdrometer. *J. Atmos. Oceanic Technol.,* **22,** 1004.

——, A. B. White, K. S. Gage, and F. M. Ralph, 2007: Vertical structure of precipitation and related microphysics observed by NOAA profilers and TRMM during NAME 2004. *J. Climate,* **20,** 1693–1712.

Zrnić, D. S., 1975: Simulation of weatherlike Doppler spectra and signals. *J. Appl. Meteor.,* **14,** 619–620.